Direct Flux Vector Control of Synchronous Motor Drives: A Small-Signal Model for Optimal Reference Generation

Direct Flux Vector Control of Synchronous Motor Drives: A Small-Signal Model for Optimal Reference Generation

Anantaram Varatharajan, Gianmario Pellegrino, *Senior Member, IEEE,* and Eric Armando, *Senior Member, IEEE,*

***Abstract*—A novel Direct Flux Vector Control (DFVC) scheme is presented based on the real-time use of the motor small-signal model for optimal reference generation without pre-processed look-up tables (LUTs). The control scheme is valid for Reluctance- and PM-Synchronous machines. The stator flux magnitude and the load angle are the controlled variables and the optimal reference values respecting maximum torque per ampere (MTPA), maximum torque per volts (MTPV), voltage and current limit conditions are computed in real-time from the small-signal model. Analytical expressions of MTPA and MTPV criteria are derived to enable online adaptation according to the small-signal approximation of the motor model. The motor parameters reside in the flux-map LUTs used in the flux observer; besides that, no additional tables are necessary. Furthermore, online parameter adaptation is proposed to further improve torque tracking accuracy against flux-map LUTs errors. The feasibility of proposed scheme is demonstrated through experiments on a 1.1. kW synchronous reluctance (SyR) machine test-bench. The proposed control scheme simplifies the implementation and calibration of the DFVC, while improving its MTPV control and its roughness against model parameter errors. Prospective fields of application are spindle and traction drives.**

***Index Terms*—Direct flux vector control, small-signal model, flux-weakening, parameter adaptation, optimal reference.**

I. Introduction

Synchronous machines can be designed to possess high torque density and good flux-weakening capability for large constant-power speed range [1]. Operations beyond rated speed finds importance in industrial applications, traction and home appliances.

The commonly used current vector control (CVC) schemes are implemented in the synchronous rotor dq coordinates where the reference current $\boldsymbol{i}^*_{dq}$ is a function of commanded torque and operating speed, fetched from a pre-processed lookup tables (LUTs) [2], [3]. An additional regulator can be used for the voltage limit to induce flux-weakening at high speeds in [4]–[7]. As rotor position is integral to CVC, the maximum torque per volt (MTPV) operations become very sensitive as small errors in rotor position can result in torque reversals. Direct torque control (DTC) is a classical technique known for its fast dynamic performance and robustness [8]. The DTC inherently facilitates flux-weakening operations due to the direct control of stator flux linkage [9]–[11].

The direct flux vector control (DFVC) is a field-oriented control in stator flux reference coordinates that combines the merits of CVC and DTC with constant switching frequency and straightforward current limitation [12]–[15]. The choice of controlled variables, stator flux magnitude λ and the quadrature torque producing current i_τ, facilitate extending operation to flux-weakening and MTPV limits. The optimal stator flux magnitude of a synchronous machine is determined by the maximum torque per ampere (MTPA) law and the voltage limit while the maximum achievable torque is determined by the current and the MTPV limit. The DFVC principle applies to PM- and Reluctance-Synchronous machine drives in general manner [14].

A model-based DFVC is reported in [16] with deadbeat-type solution. Conventionally, the stator flux oriented controllers are of proportional-integral (PI) type. However, the torque producing current loop is nonlinear due to which the dynamics become a function of the operating point. A nonlinear transformation matrix is proposed in [17] to decouple and achieve constant bandwidth of the control loops. Moreover, the torque producing current loop of DFVC approaches singularity along the MTPV trajectory where i_τ becomes uncontrollable. Hence, an inherent limitation of DFVC is the inability to operate on the MTPV limit. Therefore, a sufficient margin away from MTPV trajectory is necessary for stable operation which restricts exploiting the maximum speed-torque characteristics.

This paper proposes a new DFVC scheme where the second controlled variable, besides the stator flux linkage magnitude, is the load angle. The small-signal model of the machine under control is used to obtain decoupled linearized torque control. Moreover, the use of the load angle in place of the torque producing current circumvents the instability and permits operation at the MTPV limit.

The optimal flux magnitude and load angle references are usually retrieved from pre-processed MTPA and MTPV LUTs computed by manipulation of the flux-map LUTs of the machine under test. Alternatively, MTPA can be tracked online using signal injection [18], [19]. In this paper, the optimal flux magnitude and load angle references are calculated using the small-signal approximation of the motor model, without pre-processed LUTs.

Torque accuracy and the respect of control trajectories (MTPA, MTPV, voltage and current limits) of the proposed control scheme rely on the accurate knowledge of the motor

This work was supported by the Power Electronics Innovation Center (PEIC) of Politecnico di Torino, Italy. *(Corresponding author: Anantaram Varatharajan)*

A. Varatharajan, G. Pellegrino and E. Armando are with the Department of Energy, Politecnico di Torino, Turin 10129, Italy. (email: anantaram.varatharajan@polito.it; gianmario.pellegrino@polito.it; eric.armando@polito.it)

flux-map LUTs, contributing to the flux observer. These are normally obtained through experimental identification with a dedicated test-bench as reported in [20]; several self-commissioning techniques have been proposed [21]–[24]. However, in the presence of an erroneous flux-map LUTs, the optimal operation and efficiency can be compromised. Hence, the proposed optimal reference is supplemented with an online adaptation scheme for accurate stator flux estimation.

In Section II, the MTPA and MTPV criteria are analytically formulated in terms of the auxiliary-flux and auxiliary-current vector, respectively. Section III presents the proposed DFVC with small-signal based optimal reference generation. The main contributions of this work, in Sections III and IV, are enumerated as follows:

1) The controlled variables are the stator flux magnitude λ and the load angle δ in a linearized decoupled torque control that mitigates the instability and is capable of operation on the MTPV trajectory.
2) Online computation of the optimal control set-point, respecting MTPA, MTPV, current and voltage limits, i.e., besides the flux-map LUTs, no additional LUTs are necessary.
3) Furthermore, a stator flux adaptation is developed to suppress errors in inaccurate flux-map LUTs. Hence, unlike the off-line computed MTPA table, the proposed optimal tracking is more resilient to errors in flux-map LUTs.

Section V presents the experimental validation on a 1.1 kW synchronous reluctance (SyR) motor and Section VI concludes the paper. Although the validation is limited to the SyR machine case, the proposed concepts are also valid in general for PM-Synchronous motor drives.

II. Synchronous Machine Model

The electrical rotor position is θ and the electrical angular speed is $\omega = s\,\theta$ where s is the differential operator $\frac{\mathrm{d}}{\mathrm{d}t}$. Estimated vectors are represented by the superscript $\hat{}$. The orthogonal rotational matrix is $\mathbf{J} = \left[\begin{smallmatrix} 0 & -1 \\ 1 & 0 \end{smallmatrix}\right]$ and $\mathbf{I}$ is the identity matrix.

Real space vectors will be used; for example, the stator current is $\boldsymbol{i}_{dq} = [i_d, i_q]^{\mathrm{T}}$ where i_d and i_q are the vector components in rotor reference frame. Space vectors in the stationary reference frame are denoted by subscript $\alpha\beta$. Note that the convention of a SyR machine is followed, i.e, d-axis is defined along the maximum inductance path. The symbols and notations in the dq rotor and the $f\tau$ stator flux oriented reference frames are shown in Fig. 1.

A. Mathematical Model in dq Reference Frame

The voltage equation of a synchronous machine in rotor reference frame is expressed as

$$s\,\boldsymbol{\lambda}_{dq} = \boldsymbol{v}_{dq} - R_s \boldsymbol{i}_{dq} - \omega\,\mathbf{J}\,\boldsymbol{\lambda}_{dq} \tag{1}$$

where R_s is the stator resistance and $\boldsymbol{\lambda}_{dq}$ is the stator flux linkage. The incremental inductance is defined as

$$\boldsymbol{L}_\partial = \frac{\partial \boldsymbol{\lambda}_{dq}}{\partial \boldsymbol{i}_{dq}} = \begin{bmatrix} l_d & l_{dq} \\ l_{dq} & l_q \end{bmatrix} \tag{2}$$

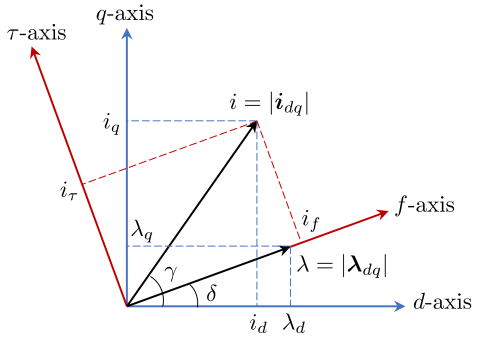

Fig. 1. Illustration of symbols and notations in the dq rotor and $f\tau$ stator flux oriented reference frames.

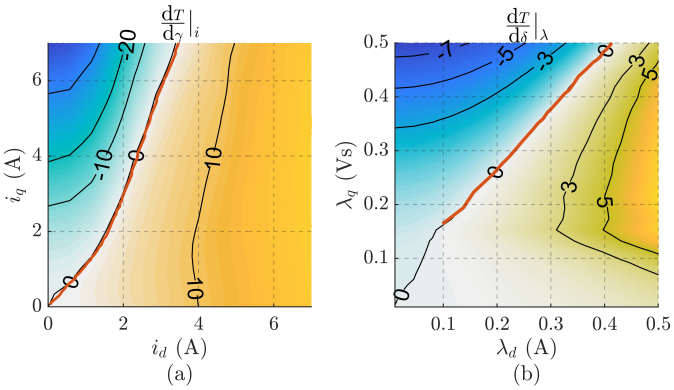

Fig. 2. (a) Contour of derivative of torque w.r.t current angle (4) where the red line is the MTPA trajectory of SyR motor under test; (b) Contour of derivative of torque w.r.t load angle (7) where the red line is the MTPV trajectory.

where l_d, l_q represents the incremental inductance along direct d and quadrature q axis, respectively, while l_{dq} is the cross-saturation term. All quantities are functions of $\boldsymbol{i}_{dq}$.

The electromagnetic torque is given by

$$T = \frac{3p}{2}\,\boldsymbol{i}_{dq}^{\mathrm{T}}\,\mathbf{J}\,\boldsymbol{\lambda}_{dq} \tag{3}$$

where p is the number of pole pairs.

B. Analytical Expression of the MTPA Law

Let γ denote the current angle. The change of torque w.r.t current angle for a given current amplitude $i = |\boldsymbol{i}_{dq}|$ is computed as [25]

$$\begin{aligned} \frac{\mathrm{d}T}{\mathrm{d}\gamma}\Big|_i &= \frac{3p}{2}\left(\frac{\mathrm{d}\boldsymbol{i}_{dq}}{\mathrm{d}\gamma}^{\mathrm{T}}\,\mathbf{J}\,\boldsymbol{\lambda}_{dq} + \boldsymbol{i}_{dq}^{\mathrm{T}}\,\mathbf{J}\,\frac{\mathrm{d}\boldsymbol{\lambda}_{dq}}{\mathrm{d}\gamma}\right) \\ &= \frac{3p}{2}\left(\boldsymbol{\lambda}_{dq}^{a}\right)^{\mathrm{T}}\mathbf{J}\,\boldsymbol{i}_{dq} \end{aligned} \tag{4}$$

where the auxiliary-flux vector $\boldsymbol{\lambda}_{dq}^{a}$ is defined as

$$\boldsymbol{\lambda}_{dq}^{a} = \mathbf{J}\,\boldsymbol{\lambda}_{dq} - \boldsymbol{L}_\partial\,\mathbf{J}\,\boldsymbol{i}_{dq}. \tag{5}$$

The contours of (4) in the dq current plane for the SyR motor under test are shown in Fig. 2(a); the MTPA trajectory is coincident with the zero locus. The MTPA law is defined as

$$\frac{\mathrm{d}T}{\mathrm{d}\gamma}\Big|_i = 0 \quad \Rightarrow \quad \left(\boldsymbol{\lambda}_{dq}^{a}\right)^{\mathrm{T}}\mathbf{J}\,\boldsymbol{i}_{dq} = 0. \tag{6}$$

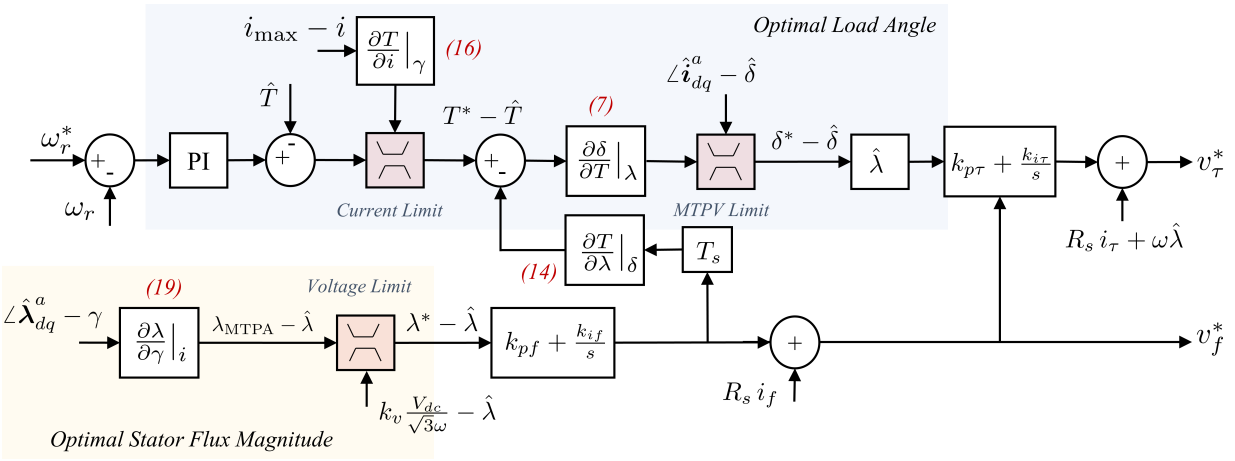

Fig. 3. Overview of the proposed flux vector control system. The model-based optimal reference generation blocks highlight the MTPA flux adaptation with voltage-limited flux reference (yellow area), current-limited torque reference and MTPV-limited load angle reference (blue area). Note that no MTPA, MTPV, flux-weakening or torque saturation LUTs are employed. The equation numbers of the small-signal expressions are shown in red.

The expression (6) dictates that the MTPA criterion is respected *if and only if* the stator current is in phase with the auxiliary-flux vector, i.e., $\gamma_{\text{MTPA}} = \angle \boldsymbol{\lambda}^a_{dq}$.

C. Analytical Expression of the MTPV Law

Let δ denote the load angle. Then, the change of torque w.r.t load angle for a given flux amplitude $\lambda = |\boldsymbol{\lambda}_{dq}|$ is computed as

$$\begin{aligned}\frac{\mathrm{d}T}{\mathrm{d}\delta}\Big|_\lambda &= \frac{3p}{2}\left(\frac{\mathrm{d}\boldsymbol{i}_{dq}}{\mathrm{d}\delta}^{\mathrm{T}} \mathbf{J}\,\boldsymbol{\lambda}_{dq} + \boldsymbol{i}_{dq}^{\mathrm{T}}\mathbf{J}\frac{\mathrm{d}\boldsymbol{\lambda}_{dq}}{\mathrm{d}\delta}\right) \\ &= \frac{3p}{2}\boldsymbol{\lambda}_{dq}^{\mathrm{T}}\mathbf{J}\,\boldsymbol{i}^a_{dq} \end{aligned} \tag{7}$$

where the auxiliary-current vector $\boldsymbol{i}^a_{dq}$ is defined as

$$\boldsymbol{i}^a_{dq} = \mathbf{J}\,\boldsymbol{i}_{dq} - \boldsymbol{L}_\partial^{-1}\mathbf{J}\,\boldsymbol{\lambda}_{dq}. \tag{8}$$

The contours of (7) in dq flux plane for the SyR motor under test is shown in Fig. 2(b); the MTPV trajectory is coincident with the zero locus. The MTPV law is defined as

$$\frac{\mathrm{d}T}{\mathrm{d}\delta}\Big|_\lambda = 0 \quad \Rightarrow \quad \boldsymbol{\lambda}_{dq}^{\mathrm{T}}\mathbf{J}\,\boldsymbol{i}^a_{dq} = 0. \tag{9}$$

The expression (9) dictates that MTPV law is respected *if and only if* the auxiliary-current is in phase with the stator flux vector, i.e., $\delta_{\text{MTPV}} = \angle \boldsymbol{i}^a_{dq}$.

III. Proposed DFVC Control System

The proposed DFVC control system uses the stator flux magnitude λ and the load angle δ as the controlled variables for the ease of flux-weakening implementation and stability under MTPV operation. The analytical expressions of MTPA and MTPV laws derived in the preceding section are used in computing the model-based optimal reference.

An overview of the control system is shown in Fig. 3. The stator flux magnitude for the MTPA condition is determined from the current angle and the phase of the auxiliary-flux vector using a small-signal model and is limited by the voltage and the operating speed as highlighted in the yellow area in Fig. 3. The optimal load angle is regulated to minimize the torque control error using a small-signal model where the torque reference is limited by the maximum permissible current. In addition, the perturbation in torque brought about by the variations in the stator flux magnitude is compensated with a small signal model as shown in the blue area in Fig. 3. The following subsections delve deeper into the design of the small-signal model.

A. Machine Dynamics in the Stator Flux Reference

The stator flux oriented reference frame is denoted by the subscript $f\tau$ where the stator flux linkage is aligned along the f-axis, i.e.,

$$\boldsymbol{\lambda}_{f\tau} = \begin{bmatrix}\lambda \\ 0\end{bmatrix} = \mathrm{e}^{-\delta\mathbf{J}}\,\boldsymbol{\lambda}_{dq}. \tag{10}$$

The voltage equation of a synchronous machine in stator flux oriented reference frame is expressed as

$$\begin{bmatrix} s\lambda \\ \lambda\, s\delta \end{bmatrix} = \boldsymbol{v}_{f\tau} - R_s\,\boldsymbol{i}_{f\tau} - \omega\mathbf{J}\,\boldsymbol{\lambda}_{f\tau}. \tag{11}$$

The electromagnetic torque is a function of the stator flux magnitude and the load angle. Analogous to the DTC in principle, the torque is controlled in the proposed scheme by regulating the load angle. The optimal reference state variables, λ^* and δ^*, are computed from the small-signal model-based scheme as discussed in the following sections.

B. Optimal Load Angle: Reference Torque Tracking

For a given stator flux magnitude, the load angle is regulated to track the reference torque. The maximum achievable torque is determined by the current and the MTPV limits.

The small-signal torque perturbation is expressed as the functions of the load angle and the stator flux magnitude as

$$\mathrm{d}T = \frac{\partial T}{\partial \delta}\Big|_\lambda \mathrm{d}\delta + \frac{\partial T}{\partial \lambda}\Big|_\delta \mathrm{d}\lambda \tag{12}$$

where the derivative of torque w.r.t load angle is derived in the MTPV formulation as (7). Manipulating, the load angle

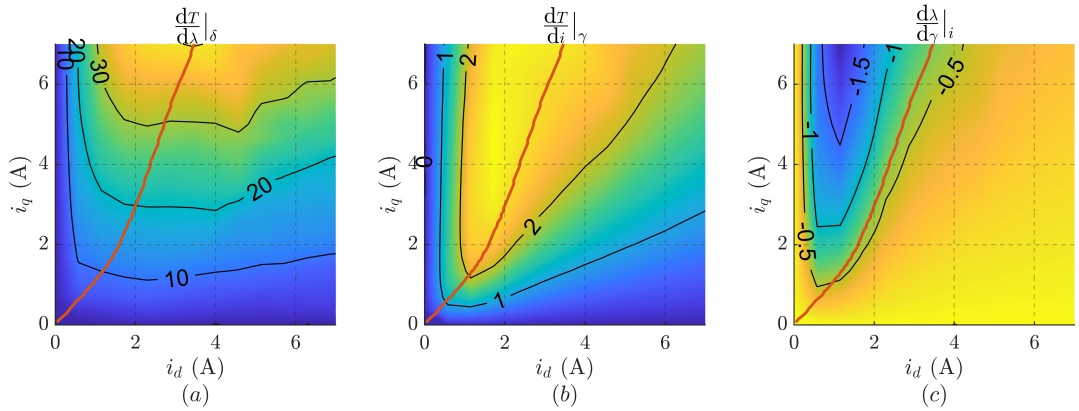

Fig. 4. (a) Contour of derivative of stator flux magnitude w.r.t current angle in A for the MTPA flux adaptation; (b) Contour of derivative of torque w.r.t stator current magnitude in Vs for the adaptive torque limit computation respecting current limitation; (c) Contour of derivative of torque w.r.t stator flux magnitude in Vs for the reference load angle computation.

reference is computed from the discrepancy between reference and estimated torque as

$$\delta^* = \hat{\delta} + \frac{\mathrm{d}\delta}{\mathrm{d}T}\Big|_\lambda \cdot \left(T^* - \hat{T} - \frac{\partial T}{\partial \lambda}\Big|_\delta \mathrm{d}\lambda\right) \tag{13}$$

where the change in flux magnitude is computed from the reference voltage as $\mathrm{d}\lambda = T_s\,(v_f^* - R_s\,i_f)$ (T_s is the control period), illustrated in Fig. 3. The derivative of torque w.r.t load angle (7) reduces to zero along the MTPV trajectory as shown in Fig. 2(b). As the expression (13) uses the inverse of (7), care must to taken for operation in the vicinity of the MTPV limit; in practice, a minimum value (≈1) is imposed on (7).

The excursion of stator flux magnitude for MTPA adaptation introduces perturbations in torque; it is compensated in (13) where the derivative of torque w.r.t stator flux is given by

$$\frac{\partial T}{\partial \lambda}\Big|_\delta = \frac{3p}{2}\frac{1}{\lambda}\left(\boldsymbol{L}_\partial^{-1}\boldsymbol{\lambda}_{dq} + \boldsymbol{i}_{dq}\right)^{\mathrm{T}}\mathbf{J}\,\boldsymbol{\lambda}_{dq}. \tag{14}$$

Having the dimension A, the contour of the gain (14) is shown in Fig. 4(a); it is worth pointing out that this gain maximizes along the MTPV trajectory in the dq flux plane.

C. Optimal Load Angle: Current Limitation

The permissible maximum stator current $i_{\max}$ limits the torque reference that is analytically expressed as an adaptive torque limit as

$$T_{max}^i = \hat{T} + \frac{\partial T}{\partial i}\Big|_\gamma \cdot \left(i_{max} - i\right) \tag{15}$$

where $\hat{T}$ is the estimated torque from the observed stator flux and measured current. The derivative of torque w.r.t stator current magnitude at a given current angle is expressed as

$$\begin{aligned}\frac{\partial T}{\partial i}\Big|_\gamma &= \frac{3p}{2}\left(\frac{\boldsymbol{i}_{dq}^{\mathrm{T}}}{i}\mathbf{J}\,\boldsymbol{\lambda}_{dq} + \boldsymbol{i}_{dq}^{\mathrm{T}}\mathbf{J}\,\boldsymbol{L}_\partial\,\frac{\boldsymbol{i}_{dq}}{i}\right)\\ &= \frac{3p}{2}\,\frac{\boldsymbol{i}_{dq}^{\mathrm{T}}}{i}\,\mathbf{J}\left(\boldsymbol{\lambda}_{dq} + \boldsymbol{L}_\partial\,\boldsymbol{i}_{dq}\right).\end{aligned} \tag{16}$$

Fig. 4(b) shows the contour of the gain (16) for the motor under test; it is worth pointing out that the gain (16) is a representative of the torque factor (Nm/A) with dimension Vs, being maximum along the MTPA trajectory. The magnitude of torque reference T^* is limited to T_{max}^i.

D. Optimal Load Angle: MTPV Limitation

The reference load angle δ^* is limited by the phase of auxiliary-current vector to respect the MTPV limitation as

$$\delta_{max} = |\angle\hat{\boldsymbol{i}}_{dq}^a| \tag{17}$$

where the estimated auxiliary-current vector $\hat{\boldsymbol{i}}_{dq}^a$ is computed from the observed stator flux.

E. Optimal Stator Flux Magnitude: MTPA Criterion

The optimal stator flux magnitude is designed to comply with the MTPA law for operations under the rated speed and with the voltage limit (flux-weakening) for operations over the rated speed.

Following (6), the MTPA condition is found by imposing the phase of the auxiliary-flux vector as the current angle. The estimated auxiliary-flux $\hat{\boldsymbol{\lambda}}_{dq}^a$ is computed from the observed stator flux described in Section IV-A. Thus, the stator flux magnitude for the MTPA condition λ_{MTPA} is calculated as

$$\lambda_{\mathrm{MTPA}} = \hat{\lambda} + \frac{\partial \lambda}{\partial \gamma}\Big|_i \cdot \left(\angle\hat{\boldsymbol{\lambda}}_{dq}^a - \gamma\right) \tag{18}$$

where the derivative of stator flux w.r.t current angle at a given current magnitude is a gain, expressed as

$$\frac{\partial \lambda}{\partial \gamma}\Big|_i = \frac{1}{\lambda}\,\hat{\boldsymbol{\lambda}}_{dq}^{\mathrm{T}}\,\boldsymbol{L}_\partial\,\mathbf{J}\,\boldsymbol{i}_{dq}. \tag{19}$$

Fig. 4(c) is the contour plot of the gain (19) with dimension Vs for the SyR motor under test. It is observed to vary little along the MTPA trajectory and could be replaced with a constant to decrease computational load.

F. Optimal Stator Flux Magnitude: Voltage Limitation

The stator flux magnitude is limited by the voltage as a function of operating speed. The maximum flux magnitude is given by

$$\lambda_{max} = k_v\,\frac{V_{dc}}{\sqrt{3}\,\omega} \tag{20}$$

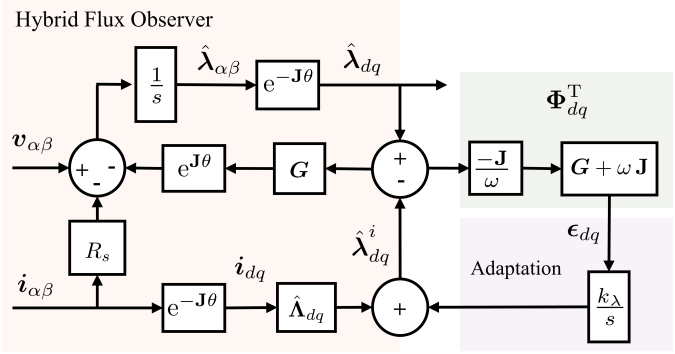

Fig. 5. Hybrid flux observer in stationary reference frame and the projection vector approach based parameter adaptation.

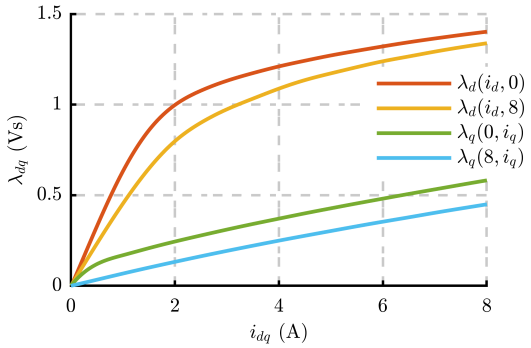

Fig. 6. Experimentally obtained flux-map of the SyR motor under test illustrating the saturation and the cross-saturation phenomenons.

where k_v is a small voltage margin ($\approx$10%). Finally, the optimal stator flux magnitude reference λ^* is the λ_{MTPA} limited by λ_{max}.

Thus, the optimal references are computed entirely relying on the small-signal model around the operating point without additional LUTs. Note that the small-signal terms (19), (16) and (14) are gains; hence, any reasonable approximation does not affect the steady-state performance.

G. Stator Flux Oriented Controller

It follows from (11) that the voltage reference can be computed with a proportional-integral (PI) regulator and feed-forward terms as

$$\boldsymbol{v}_{f\tau}^{*} = R_s\,\boldsymbol{i}_{f\tau} + \mathbf{J}\,\omega\,\hat{\boldsymbol{\lambda}}_{f\tau} + \left[\boldsymbol{K}_p + \frac{\boldsymbol{K}_i}{s}\right]\begin{bmatrix}\lambda^* - \hat{\lambda}\\ \hat{\lambda}(\delta^* - \hat{\delta})\end{bmatrix} \tag{21}$$

where $\hat{\boldsymbol{\lambda}}_{f\tau}$ is the observed stator flux in Section IV-A, the proportional $\boldsymbol{K}_p$ and integral $\boldsymbol{K}_i$ gains are diagonal matrices with terms k_{pf}, $k_{p\tau}$ and k_{if}, $k_{i\tau}$, respectively. The f-axis gains are tuned for critical damping at $s = -\Omega_f$ as

$$k_{pf} = 2\,\Omega_f \qquad k_{if} = \Omega_f^2. \tag{22}$$

The τ-axis gains are tuned in a similar fashion for critical damping at $s = -\Omega_\tau$. The torque loop is recommended to be faster than the flux loop to curtain overshoot in torque during transients. Moreover, the PI regulator in the f-axis is limited to one third of the rated voltage.

Provided that the torque reference is translated into corresponding λ and δ references, and that the feed-forward terms are accurate, the controller (21) is linear and decoupled.

IV. Adaptive Flux Observer

The flux-map LUTs can be prone to errors that introduce inaccuracies in flux estimation and adversely affects the small-signal computations for the optimal operating point. Hence, the hybrid flux observer (HFO) in use is supplemented with parameter adaptation. The comprehensive hybrid flux observer with adaptation for parameter error is shown in Fig. 5.

A. Hybrid Flux Observer

Let $\boldsymbol{\Lambda}_{dq}$ denote the flux-map LUTs of the machine under test such that $\boldsymbol{\lambda}_{dq}^{i} = \boldsymbol{\Lambda}_{dq}(\boldsymbol{i}_{dq})$ where $\boldsymbol{\lambda}_{dq}^{i}$ denotes the current-model flux estimate. Fig. 6 shows the flux-map of SyR machine under test that is experimentally identified with constant speed test reported in [20]. The state equation of the flux observer in stationary reference frame is defined as

$$s\hat{\boldsymbol{\lambda}}_{\alpha\beta} = \boldsymbol{v}_{\alpha\beta} - R_s\boldsymbol{i}_{\alpha\beta} + \mathrm{e}^{\mathbf{J}\theta}\,\boldsymbol{G}\left(\boldsymbol{\lambda}_{dq}^{i} - \hat{\boldsymbol{\lambda}}_{dq}\right) \tag{23}$$

where $\hat{\boldsymbol{\lambda}}_{\alpha\beta}$ is the observed flux and $\boldsymbol{G}$ is a 2×2 gain matrix. The observed torque is computed using the observed stator flux as

$$\hat{T} = \frac{3p}{2}\,\boldsymbol{i}_{\alpha\beta}^{\mathrm{T}}\,\mathbf{J}\,\hat{\boldsymbol{\lambda}}_{\alpha\beta}. \tag{24}$$

In this work, a diagonal matrix $\boldsymbol{G} = g\,\mathbf{I}$ is used. For electrical speeds above g rad/s, the voltage-model (back-emf integration) prevails. The observer is called hybrid to signify the combination of voltage and current-models. Typically, it is common to set the gain g between 0.1-0.2 p.u. of the rated speed.

B. Adaptation under Parameter Errors

Let $\hat{\boldsymbol{\Lambda}}_{dq}$ denote the flux-map LUTs accounting for parameter error. Then, the error in the current-model flux estimate $\tilde{\boldsymbol{\lambda}}_{dq}^{i}$ is given by

$$\tilde{\boldsymbol{\lambda}}_{dq}^{i} = \boldsymbol{\Lambda}_{dq}(\boldsymbol{i}_{dq}) - \hat{\boldsymbol{\Lambda}}_{dq}(\boldsymbol{i}_{dq}). \tag{25}$$

The flux observer state equation (23) is transformed to the dq reference for analysis purposes as

$$s\hat{\boldsymbol{\lambda}}_{dq} = \boldsymbol{v}_{dq} - R_s\boldsymbol{i}_{dq} - \omega\,\mathbf{J}\,\hat{\boldsymbol{\lambda}}_{dq} + \boldsymbol{G}\left(\hat{\boldsymbol{\lambda}}_{dq}^{i} - \hat{\boldsymbol{\lambda}}_{dq}\right). \tag{26}$$

It follows from (1) and (26) that the discrepancy between the observed flux and the current-model flux can be expressed as

$$\hat{\boldsymbol{\lambda}}_{dq} - \hat{\boldsymbol{\lambda}}_{dq}^{i} = \left(s\mathbf{I} + \boldsymbol{G} + \omega\mathbf{J}\right)^{-1}\left(s\mathbf{I} + \omega\mathbf{J}\right)\tilde{\boldsymbol{\lambda}}_{dq}^{i}. \tag{27}$$

At steady-state conditions ($s = 0$), the former expression simplifies to

$$\hat{\boldsymbol{\lambda}}_{dq} - \hat{\boldsymbol{\lambda}}_{dq}^{i}\big|_{s=0} = \left(\boldsymbol{G} + \omega\mathbf{J}\right)^{-1}\omega\mathbf{J}\,\tilde{\boldsymbol{\lambda}}_{dq}^{i}. \tag{28}$$

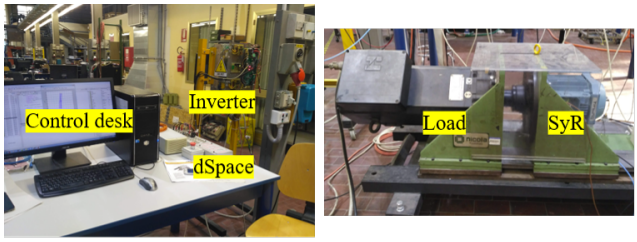

Fig. 7. Experimental Setup of 1.1 kW SyR motor under test on a dSPACE DS1103 control platform at a sampling frequency of 10 kHz.

This leads to the error function of nature

$$\boldsymbol{\epsilon}_{dq} = \boldsymbol{\Phi}_{dq}^{\mathrm{T}} \left(\hat{\boldsymbol{\lambda}}_{dq} - \hat{\boldsymbol{\lambda}}_{dq}^{i} \right) \tag{29}$$

where the 2×2 matrix $\boldsymbol{\Phi}_{dq}^{\mathrm{T}}$ is given by

$$\boldsymbol{\Phi}_{dq}{}^{\mathrm{T}} = \frac{-\mathbf{J}}{\omega} \left(\boldsymbol{G} + \mathbf{J}\, \omega \right). \tag{30}$$

It is noted that the current-model flux error signal $\boldsymbol{\epsilon}_{dq}$ is equal to the parameter error in steady-state condition, i.e., $\boldsymbol{\epsilon}_{dq}\big|_{s=0} = \tilde{\boldsymbol{\lambda}}_{dq}$. An integral regulator is therefore set up to rectify the flux-map LUTs error, according to the flux estimate error function (29)-(30) as

$$\hat{\boldsymbol{\lambda}}_{dq}^{i} = \hat{\boldsymbol{\Lambda}}_{dq}(\boldsymbol{i}_{dq}) + \frac{k_\lambda}{s}\, \boldsymbol{\epsilon}_{dq} \tag{31}$$

where k_λ is integral gain.

Note that the proposed adaption mitigates error in the flux estimation but error in incremental inductance remains. If needed, this can be mitigated with high frequency signal injection techniques although not viable at high speeds operation. Dealing with the proposed control scheme, flux adaptation (31) guarantees that the steady-state value of controlled torque is accurately tracked, though the effect of parameter detuning during torque transients is unavoidable.

V. Experimental Results

The proposed DFVC with adaptation is validated experimentally on a 1.1 kW SyR motor on a dSPACE DS1103 control platform running at a sampling frequency of 10 kHz. A picture of the setup is shown in Fig. 7. The parameters of the SyR motor under test are tabulated in Table I.

The flux observer gain is $g = 2\,\pi \cdot 10$ rad/s. The speed PI and the stator flux controllers are tuned for critical damping at $s = -2\pi \cdot 1.5$ rad/s, $\Omega_\tau = 2\pi \cdot 150$ rad/s and $\Omega_f = 2\pi \cdot 30$ rad/s. The flux adaptation gain is $k_\lambda = 2\pi \cdot 5$ rad/s.

The incremental inductance matrix $\boldsymbol{L}_\partial$ is retrieved from the flux-map LUTs in real-time; as an example:

$$\hat{l}_d(\boldsymbol{i}_{dq}) = \frac{\hat{\boldsymbol{\Lambda}}_d(i_d + \delta i_d, i_q) - \hat{\boldsymbol{\Lambda}}_d(i_d, i_q)}{\delta i_d} \tag{32}$$

where δi_d is a small value (≈ 10 mA). The other incremental inductances are computed in a similar fashion.

A. Speed Step Response

A step speed in reference is commanded at standstill to 1.75 p.u., $\omega_r^* = 0 \rightarrow 2625$ rpm, at $t = 0$ s as shown in Fig. 8. A 50% overload in current is permitted in this test, i.e., $i_{max} = 1.5 \cdot \sqrt{2}\, I_n$ A. The different stages of the result are analyzed in time segments:

TABLE I
Motor Parameters

Parameters	Symbol	Values	Units
Rated power	P_n	1.1	kW
Rated voltage	V_n	340	V
Rated speed	ω_n	1500	rpm
Rated current	I_n	2.9	A
Rated torque	T_n	7.1	Nm
Pole pairs	p	2	-
Stator resistance	R_s	6.2	Ω
Shaft inertia	J	0.04	kgm^2

1) MTPA Operation - $0 < t \leq 0.4$ s: In response to the step in speed reference, the control operates at the maximum torque $\hat{T} = T_{max}^i$ in (15), limited by the current i_{max}. The quantity T_{max}^i for $t < 0$ s is discerned to be ≈ 6 Nm but this is irrelevant as it is computed using the small-signal model at no-load. The MTPA operation is evidenced by the current angle coincident with the phase of auxiliary-flux vector, i.e., $\gamma = \angle \boldsymbol{\lambda}_{dq}^a$, recalling the MTPA definition (6). This is further validated with the MTPA LUTs-based stator current magnitude which is observed to be coherent with the measured $|\boldsymbol{i}_{dq}|$ in this time-span.

2) Maximum Current Locus - $0.4 < t \leq 0.85$ s: The time $t = 0.4$ s marks the onset of the flux-weakening region due to voltage limit at the speed $\omega_r = 1100$ rpm (0.73 p.u). The flux-weakening is enforced prior to the rated speed due to the permitted 50% overload in the current. As the speed increases, the control traverses along the maximum current locus where the stator current magnitude i is constant, with progressively decreasing torque output.

3) MTPV Limit - $t > 0.85$ s: The intersection of the maximum current locus with the MTPV trajectory occurs at $t = 0.85$ s. For speeds beyond, the maximum torque is dictated by the MTPV limit; the MTPV operation is evidenced by the observed load angle coincident with the phase of auxiliary-current vector, i.e., $\hat{\delta} = \angle \boldsymbol{i}_{dq}^a$, recalling the MTPV definition (2). Furthermore, the achievable torque at the speed 1.75 p.u is observed to be about 35% of rated torque (≈ 2.5 Nm). It illustrates the poor capability of SyR machines to operate in the deep flux-weakening regions.

The three small-signal gains in Fig. 8, referring to Fig. 4, are computed for each operating point in real-time from the observed stator flux (23) and the incremental inductance (32).

B. Comparison against State-of-Art DFVC Scheme

The state-of-art DFVC with λ and i_τ as the state variables is the decoupled control with nonlinear transformation, proposed in [17]. As alluded to before, the main drawback of the state-of-art DFVC is the inability at operate at the MTPV limit. Thus, for stability reasons, a torque margin of 10% from the MTPV limit is imposed. This scheme is subjected to a similar speed step response as the former test under the same conditions, shown in Fig. 9.

The two schemes are observed to be nearly identical in the MTPA and the maximum current locus operation until $t = 0.65$ s. The imposed torque margin in Fig. 9 limits the

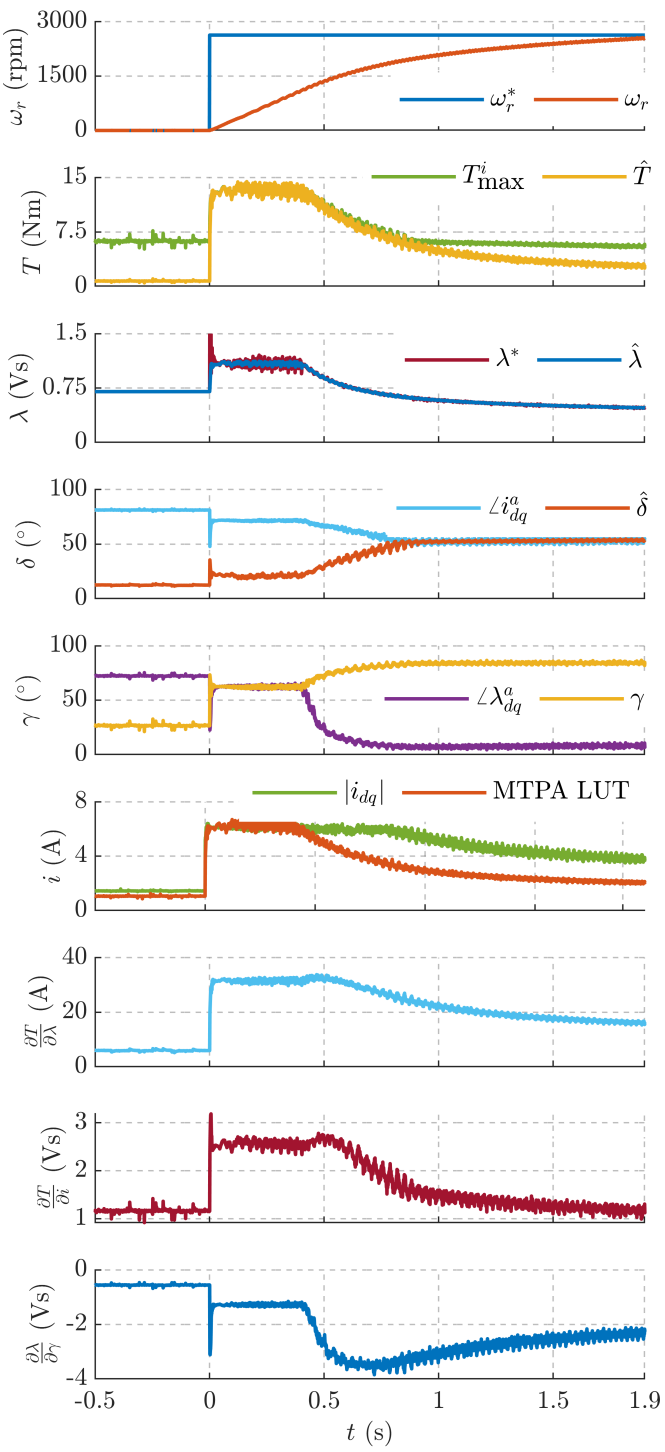

Fig. 8. Speed control of the proposed small-signal scheme with a step reference $\omega_r = 0 \rightarrow 2625$ rpm (1.75 p.u.) commanded at $t = 0$ s to illustrate the efficacy of the proposed optimal reference scheme. A 50% overload in current is allowed.

operation on the maximum current locus and forces the control into a premature MTPV operation at $t = 0.65$ s while the proposed control tracks the maximum current locus for a much longer time until $t = 0.85$ s in Fig. 8. The discernible difference between the phase of auxiliary-current and the load

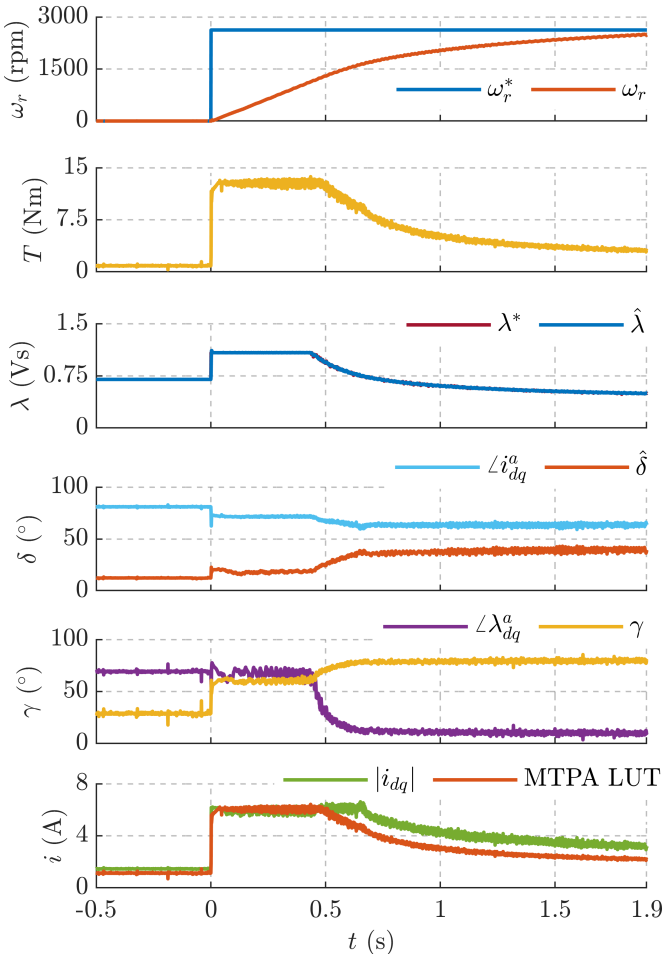

Fig. 9. Speed control of the state-of-art DFVC scheme [17] with a step reference $\omega_r = 0 \rightarrow 2625$ rpm (1.75 p.u.) commanded at $t = 0$ s. MTPV torque margin of 10% is imposed for stability. A 50% overload in current is allowed.

angle for $t > 0.65$ s, as opposed to the result in Fig. 8, suggests that the control is operating beneath the maximum achievable torque. This torque saturation below the MTPV limit increases the settling time by about 10% w.r.t to the proposal small-signal scheme in Fig. 8. This illustrates the advantage of the proposed scheme in mitigating the instability of the state-or-art DFVC at the MTPV limit. It is worth mentioning that the two schemes have comparable computational effort in terms of the turnaround time (≈40 μ s).

C. Torque Transient Response

Under the torque control mode with the speed regulated by the auxiliary drive, a step reference $T^* = 10$ Nm (1.5 p.u.) is commanded at $t = 0$ s at half the rated speed in Fig. 10(a). At the onset, the stator flux and the load angle references that are computed based on the small-signal quantities of the present operating point are initially inaccurate but converge as the operating point moves closer to the final steady-state value.

No torque overshoot is discerned; a small overshoot in load angle is observed which is due to the higher bandwidth of

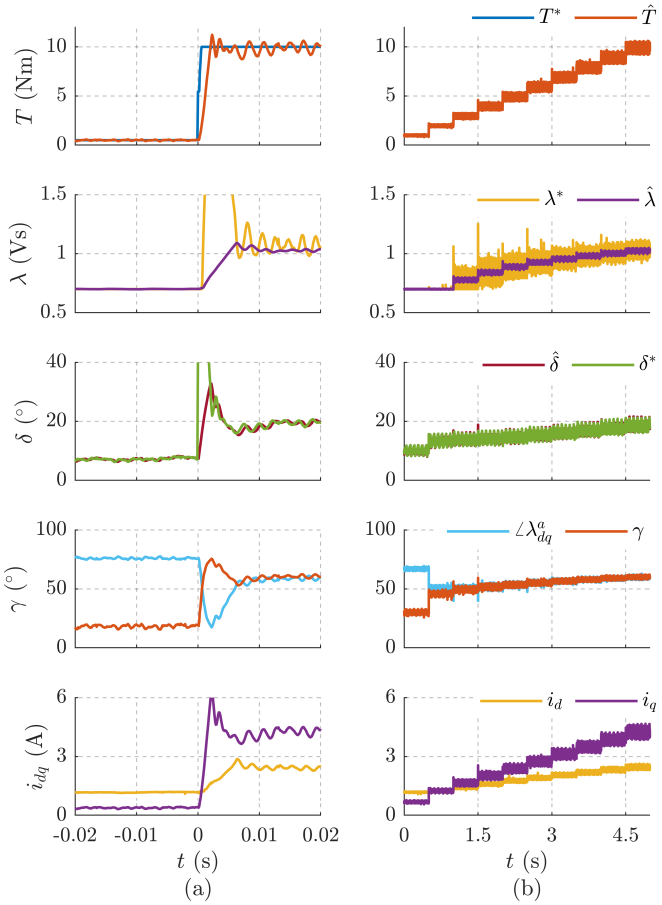

Fig. 10. (a) Torque control with a step reference $T^* = 10$ Nm (1.5 p.u.) commanded at $t = 0$ s at half 750 rpm (0.5 p.u) to illustrate the transient dynamics; (b) Torque control with a incremental reference $T^* = 1 \rightarrow 10$ Nm (1.5 p.u.) in steps of 1 Nm at 750 rpm (0.5 p.u.) to illustrate steady-state stability.

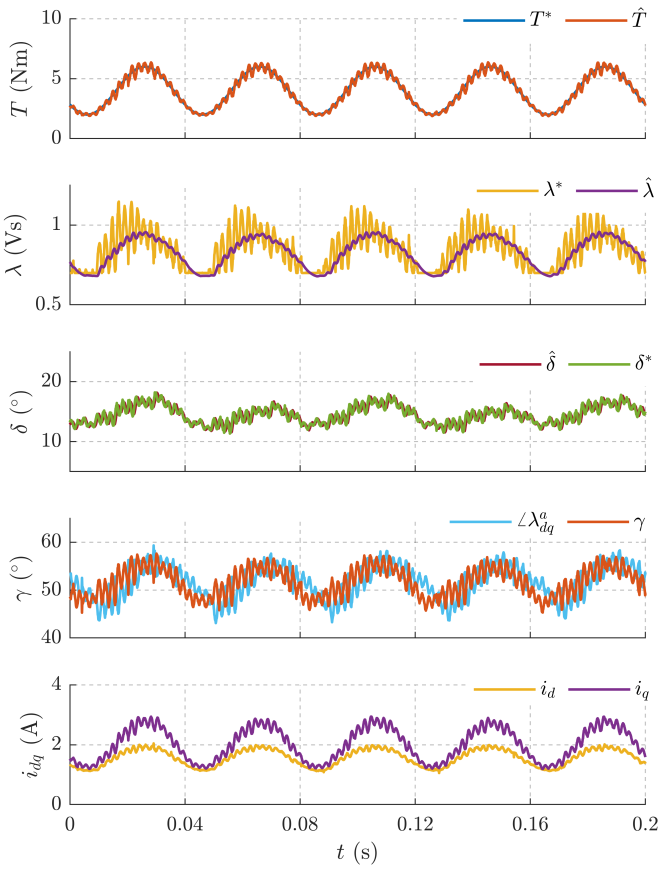

Fig. 11. Sinusoidal perturbations at 25 Hz imposed on the reference torque at 750 rpm to illustrate the dynamic MTPA tracking capability.

torque loop relative to the flux loop. The settling time of torque is about 1 ms while stator flux to MTPA condition is about 5 ms.

To ascertain steady-state stability at all torque levels, an incremental reference of $T^* = 1 \rightarrow 10$ Nm (1.5 p.u.) in steps of 1 Nm is imposed at 750 rpm (0.5 p.u.) in Fig. 10(b). The noise is attributed to the strong MMF harmonics exhibited by the motor under test; the dead-time of the inverter is compensated appropriately. The torque tracking and flux adaption for MTPA condition are validated.

D. Dynamic MTPA Tracking

The dynamic MTPA tracking capability of the drive is validated at 750 rpm in Fig. 11 with a sinusoidal perturbation in reference torque at 25 Hz. The stator flux is adapted ceaselessly to traverse along the MTPA trajectory where the current angle is observed to be coincident with the phase of auxiliary-flux vector, $\gamma = \angle\boldsymbol{\lambda}^a_{dq}$. The small high-frequency oscillations correspond to the 18^{th} harmonic of the machine under test.

E. Parameter Error Adaptation

The hybrid flux observer is susceptible to parameter errors in the flux-map LUTs, especially in the low speed regions. Hence, the validation of current-model flux adaptation is demonstrated at 0.33 p.u. (500 rpm) and at rated torque reference in Fig. 12. In the figures, the quantities T and $\angle\boldsymbol{\lambda}^a_{dq}$ are the torque and the phase of auxiliary-flux vector, respectively, computed with accurate parameters.

Any error in observed flux propagates to the observed torque $\hat{T}$ (24) and ultimately, results in a discrepancy between the reference and the actual torque. In Fig. 12, the torque estimate using the accurate flux-map is considered a good representative of the actual torque T. A 25% error in d-axis flux-map LUTs, $\hat{\lambda}^i_d = 0.75\,\lambda_d$, is considered in Fig. 12(a). While the reference torque is $T^* = 7.1$ Nm, the actual torque is $T \approx 8$ Nm which is approximately -14% error. The flux adaptation is enabled at $t = 0$ s upon which the observed and current-model flux estimates converge and accurate torque control is realized.

The flux adaptation decreases the discrepancy between the current angle and the phase of the real auxiliary-flux vector $\boldsymbol{\lambda}^a_{dq}$; however, they are not coincident because the estimated auxiliary-flux vector $\hat{\boldsymbol{\lambda}}^a_{dq}$ is susceptible to the error in the incremental inductance following (32). Thus, the flux adaptation moves the control closer to the optimal MTPA operating point though a small inaccuracy remains.

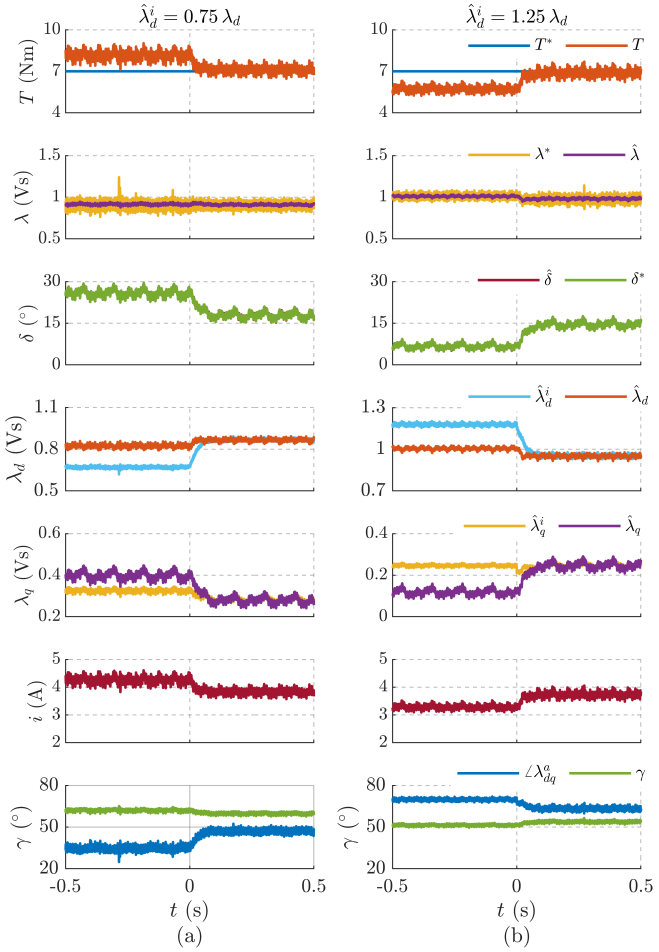

Fig. 12. Torque control under parameter error at 500 rpm (0.33 rpm) and $T^* = 7.1$ Nm (1 p.u.): (a) +25% error in d-axis flux-map LUTs, $\hat{\lambda}_d^i = 0.75\,\lambda_d$; (b) -25% error in d-axis flux-map LUTs, $\hat{\lambda}_d^i = 1.25\,\lambda_d$. The current-model flux adaptation is enabled at $t = 0$ s.

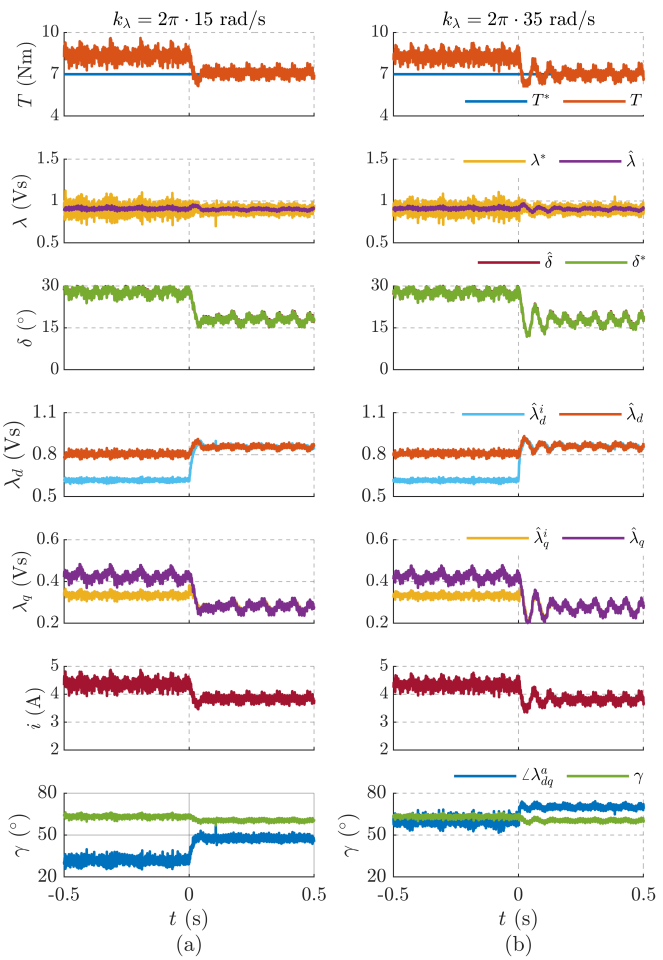

Fig. 13. Impact of the gain k_λ on the flux adaptation at +25% error in d-axis flux-map LUTs, $\hat{\lambda}_d^i = 0.75\,\lambda_d$, 500 rpm (0.33 rpm) and $T^* = 7.1$ Nm (1 p.u.): (a) $k_\lambda = 2\pi \cdot 15$ rad/s; (b) $k_\lambda = 2\pi \cdot 35$ rad/s. The current-model flux adaptation is enabled at $t = 0$ s.

Similar test at -25% error in d-axis flux-map LUTs, $\hat{\lambda}_d^i = 1.25\,\lambda_d$, is shown in Fig. 12(b) where the error between the reference and actual torque prior to flux adaptation is approximately +18%. Once the flux adaptation is enabled, the errors in stator flux and torque are mitigated. A small inaccuracy in MTPA tracking remains as seen from the discrepancy between the phase of the real auxiliary-flux (computed using accurate flux-maps) and the current angle; this is due to the error in the incremental inductance (32).

The impact of the gain k_λ on the flux adaptation is evaluated at +25% error in d-axis for values $k_\lambda = 2\pi \cdot 15$ rad/s and $k_\lambda = 2\pi \cdot 35$ rad/s in Figs. 13(a) and 13(b), respectively. It can be discerned that while 15 Hz shows good dynamics, the adaptation at 35 Hz shows under-damped oscillations. Hence, a very high k_λ is not recommended.

VI. Conclusion

The paper proposed a DFVC control with the stator flux and the load angle as the controlled variables, contrary to the conventional stator flux and the quadrature torque producing current i_τ. This choice of controlled variables circumvents the singularity problem of the i_τ current loop and permits operation on the MTPV trajectory to exploit the maximum torque-speed characteristics of the machine. Besides, the new scheme obtains linear and decoupled torque control.

The optimal stator flux and load angle references are computed from the small-signal model around the present operating point. This novelty is the primary contribution of the paper. Besides the flux-map LUTs, no additional tables are necessary. The MTPA and MTPV criteria are analytically expressed in terms of auxiliary-flux and auxiliary-current vector, respectively, to facilitate online adaptation.

Furthermore, a current-model flux adaptation is supplemented to mitigate parameter errors in flux-map LUTs. Unlike the control relying on pre-processed MTPA and MTPV LUTs, an improved optimal operation is feasible under flux adaptation; thus, the proposed scheme becomes more resilient to parameter error. In addition, mitigating error in flux estimation assists in accurate torque control.

The proposed DFVC scheme with the small-signal based optimal reference scheme and flux adaptation is experimentally validated on a 1.1 kW SyR motor test-bench.

REFERENCES

[1] N. Bianchi, S. Bolognani, and B. J. Chalmers, "Salient-rotor PM synchronous motors for an extended flux-weakening operation range," *IEEE Transactions on Industry Applications*, vol. 36, no. 4, pp. 1118–1125, 2000.

[2] B. Cheng and T. R. Tesch, "Torque feedforward control technique for permanent-magnet synchronous motors," *IEEE Transactions on Industrial Electronics*, vol. 57, no. 3, pp. 969–974, 2010.

[3] H. A. A. Awan, Z. Song, S. E. Saarakkala, and M. Hinkkanen, "Optimal Torque Control of Saturated Synchronous Motors: Plug-and-Play Method," *IEEE Transactions on Industry Applications*, p. 1, 2018.

[4] B. H. Bae, N. Patel, S. Schulz, and S. K. Sul, "New Field Weakening Technique for High Saliency Interior Permanent Magnet Motor," *Conference Record - IAS Annual Meeting (IEEE Industry Applications Society)*, vol. 2, no. 2, pp. 898–905, 2003.

[5] S. Bolognani, S. Calligaro, and R. Petrella, "Adaptive Flux-Weakening Controller for Interior Permanent Magnet Synchronous Motor Drives," *IEEE Journal of Emerging and Selected Topics in Power Electronics*, vol. 2, no. 2, pp. 236–248, 2014.

[6] V. Manzolini, D. D. Rù, and S. Bolognani, "An Effective Flux Weakening Control of a SyRM Drive Including MTPV Operation," *IEEE Transactions on Industry Applications*, vol. 55, no. 3, pp. 2700–2709, 2019.

[7] N. Bedetti, S. Calligaro, and R. Petrella, "Analytical Design and Autotuning of Adaptive Flux-Weakening Voltage Regulation Loop in IPMSM Drives With Accurate Torque Regulation," *IEEE Transactions on Industry Applications*, vol. 56, no. 1, pp. 301–313, 2020.

[8] G. S. Buja and M. P. Kazmierkowski, "Direct torque control of PWM inverter-fed AC motors - A survey," *IEEE Transactions on Industrial Electronics*, vol. 51, no. 4, pp. 744–757, 2004.

[9] C. Choi, J. Seok, and R. D. Lorenz, "Wide-Speed Direct Torque and Flux Control for Interior PM Synchronous Motors Operating at Voltage and Current Limits," *IEEE Transactions on Industry Applications*, vol. 49, no. 1, pp. 109–117, 2013.

[10] Y. Inoue, S. Morimoto, and M. Sanada, "Comparative Study of PMSM Drive Systems Based on Current Control and Direct Torque Control in Flux-Weakening Control Region," *IEEE Transactions on Industry Applications*, vol. 48, no. 6, pp. 2382–2389, 2012.

[11] X. Zhang, G. H. B. Foo, D. M. Vilathgamuwa, and D. L. Maskell, "An Improved Robust Field-Weakeaning Algorithm for Direct-Torque-Controlled Synchronous-Reluctance-Motor Drives," *IEEE Transactions on Industrial Electronics*, vol. 62, no. 5, pp. 3255–3264, 2015.

[12] H. F. Hofmann, S. R. Sanders, and A. El-Antably, "Stator-flux-oriented vector control of synchronous reluctance machines with maximized efficiency," *IEEE Transactions on Industrial Electronics*, vol. 51, no. 5, pp. 1066–1072, 2004.

[13] G. Pellegrino, E. Armando, and P. Guglielmi, "Direct flux field-oriented control of IPM drives with variable DC link in the field-weakening region," *IEEE Transactions on Industry Applications*, vol. 45, no. 5, pp. 1619–1627, 2009.

[14] G. Pellegrino, R. I. Bojoi, and P. Guglielmi, "Unified direct-flux vector control for AC motor drives," *IEEE Transactions on Industry Applications*, vol. 47, no. 5, pp. 2093–2102, 2011.

[15] G. Pellegrino, B. Boazzo, and T. M. Jahns, "Direct flux control of PM synchronous motor drives for traction applications," *2014 IEEE Transportation Electrification Conference and Expo: Components, Systems, and Power Electronics - From Technology to Business and Public Policy, ITEC 2014*, no. c, pp. 1–6, 2014.

[16] B. Boazzo and G. Pellegrino, "Model-Based Direct Flux Vector Control of Permanent-Magnet Synchronous Motor Drives," *IEEE Transactions on Industry Applications*, vol. 51, no. 4, pp. 3126–3136, 2015.

[17] H. A. A. Awan, M. Hinkkanen, R. Bojoi, and G. Pellegrino, "Stator-Flux-Oriented Control of Synchronous Motors: A Systematic Design Procedure," *IEEE Transactions on Industry Applications*, vol. 55, no. 5, pp. 4811–4820, 2019.

[18] S. Bolognani, R. Petrella, A. Prearo, and L. Sgarbossa, "Automatic Tracking of MTPA Trajectory in IPM Motor Drives Based on AC Current Injection," *IEEE Transactions on Industry Applications*, vol. 47, no. 1, pp. 105–114, 2011.

[19] Y. Lee and S.-K. Sul, "Position-Sensorless MTPA Control of IPMSM Based on High-Frequency Signal Injection," in *2019 10th International Conference on Power Electronics and ECCE Asia (ICPE 2019 - ECCE Asia)*, 2019, pp. 2562–2567.

[20] E. Armando, R. I. Bojoi, P. Guglielmi, G. Pellegrino, and M. Pastorelli, "Experimental identification of the magnetic model of synchronous machines," *IEEE Transactions on Industry Applications*, vol. 49, no. 5, pp. 2116–2125, 2013.

[21] G. Pellegrino, B. Boazzo, and T. M. Jahns, "Magnetic Model Self-Identification for PM Synchronous Machine Drives," *IEEE Transactions on Industry Applications*, vol. 51, no. 3, pp. 2246–2254, 2015.

[22] M. Hinkkanen, P. Pescetto, E. Mölsä, S. E. Saarakkala, G. Pellegrino, and R. Bojoi, "Sensorless Self-Commissioning of Synchronous Reluctance Motors at Standstill Without Rotor Locking," *IEEE Transactions on Industry Applications*, vol. 53, no. 3, pp. 2120–2129, 2017.

[23] P. Pescetto and G. Pellegrino, "Automatic Tuning for Sensorless Commissioning of Synchronous Reluctance Machines Augmented with High-Frequency Voltage Injection," *IEEE Transactions on Industry Applications*, vol. 54, no. 5, pp. 4485–4493, 2018.

[24] A. Varatharajan, P. Pescetto, and G. Pellegrino, "Sensorless Self-Commissioning of Synchronous Reluctance Machine with Rotor Self-Locking Mechanism," in *2019 IEEE Energy Conversion Congress and Exposition (ECCE)*, 2019, pp. 812–817.

[25] H. Kim, Y. Lee, S. K. Sul, J. Yu, and J. Oh, "Online MTPA Control of IPMSM for Automotive Applications Based on Robust Numerical Optimization Technique," in *2018 IEEE Transportation Electrification Conference and Expo (ITEC)*, 2018, pp. 442–447.